

# Thermodynamic, kinetic and dynamic aspects of biogas upgrading using nano-engineered grazyne

Francesc Viñes, Adrià Calzada, Pablo Gamallo\*

Departament de Ciència de Materials i Química Física, Institut de Química Teòrica i Computacional (IQTUB), Universitat de Barcelona, c/Martí i Franquès 1-11, 08028 Barcelona, Spain

## ARTICLE INFO

### Keywords:

Biogas upgrading  
Grazyne  
Density functional theory  
Molecular dynamics  
Semipermeable membranes

## ABSTRACT

Different nano-engineered grazyne have been studied as possible membranes to separate methane (CH<sub>4</sub>) from carbon dioxide (CO<sub>2</sub>) by density functional theory (DFT) and molecular dynamics (MD) computational simulations. The study tackles the process thermodynamics, kinetics, and dynamical aspects associated to the diffusion rates and selectivities in the context of biogas upgrading while comparing to other materials available in the literature. Small adsorption energy values have been obtained for three semi-permeable grazyne, with low diffusion energy barriers which severely reduce as long as the grazyne pore increases. Selectivities towards CO<sub>2</sub> permeation as large as 39 are found at high pressures for [1],[2]-grazyne, closely followed by [1],[2]-(00,2)-grazyne, posing grazyne as excellent membranes for biogas upgrading with clear advantages compared to scrubbing materials in terms of much improved selectivity, continuous workflow and an order of magnitude larger quantity of separated CO<sub>2</sub> per material gram. Present computational simulations reveal that grazyne could be able to upgrade biogas beyond 97 % (v/v) in methane, accomplishing standard worldwide government requirements.

## 1. Introduction

The concentration of greenhouse gases such as carbon dioxide (CO<sub>2</sub>) and methane (CH<sub>4</sub>) in the Earth's atmosphere are continuously increasing, being the main cause of global warming and climate change [1]. In this sense, the use of renewable energies has become a recurring topic in order to reduce the emission of greenhouse gases and, at the same time, to meet the increasing worldwide energy demands [2]. However, such technologies are still far from coping with such needs, and other options need to be considered in the meantime.

Within this context, one way of reducing the CO<sub>2</sub> emissions is optimizing the energy efficiency of existing processes. For instance, removing CO<sub>2</sub> from CH<sub>4</sub> biogas fuel streams ensures an increase in the combustion power. Actually, the presence of CO<sub>2</sub> in biogas streams significantly decreases the calorific value of the latter, to values around 15–30 MJ/Nm<sup>3</sup> when CO<sub>2</sub> is present. In this sense, finding a process to effectively eliminate CO<sub>2</sub> from the biogas mixture is of utmost importance since it would allow a better use of biogas power, laying the path for its use as substitution of fossil fuels [3]. Here, the sought purity of CH<sub>4</sub> required for its use as fuel has to be higher than 95 % (v/v) [4]. However, the extracted biogas streams feature 50–75 % (v/v) of

methane purity admixed with 25–50 % CO<sub>2</sub> [4], which makes necessary the biogas upgrading process separating CO<sub>2</sub> from CH<sub>4</sub> prior to its use as fuel. Apart from these two main components, traces of other components, such as hydrogen sulfide (H<sub>2</sub>S), ammonia, siloxane, hydrogen, water, and volatile organic compounds can be found in biomethane, which may complicate the biogas upgrading. For example, studies have shown that H<sub>2</sub>S can act as a poison for CO<sub>2</sub> sorbents, blocking the surface adsorption sites, which makes necessary to regenerate the capture material to avoid the H<sub>2</sub>S passivation, or its eventual corrosion [3].

Actually, the chemical resolution —i.e., chemical separation— of CO<sub>2</sub> from CH<sub>4</sub> is quite an intricate problem, mostly due to the fact that both molecules are chemically stable, and, consequently, quite inactive, ultimately complicating their selective chemical resolution. One of the main technologies to remove the CO<sub>2</sub> present in the mixture is the so-called amine scrubbing [3]. Studies have shown that amines have great advantages in the capture and treatment of CO<sub>2</sub>, obtaining fast absorption rates and high CO<sub>2</sub> selectivities, but, at the same time, they present problems when it comes to regenerating the material or when considering the amine degeneration [3]. Recently, transition metal carbides (TMCs) and their two-dimensional (2D) versions, MXenes, have been proposed as suited materials capable of carrying out the separation

\* Corresponding author.

E-mail address: [gamallo@ub.edu](mailto:gamallo@ub.edu) (P. Gamallo).

<https://doi.org/10.1016/j.jcou.2023.102459>

Received 2 January 2023; Received in revised form 8 March 2023; Accepted 12 March 2023

Available online 22 March 2023

2212-9820/© 2023 The Author(s). Published by Elsevier Ltd. This is an open access article under the CC BY license (<http://creativecommons.org/licenses/by/4.0/>).

of both molecules by selective adsorption of CO<sub>2</sub> [4,5]. Their use implies having the material eventually saturated by CO<sub>2</sub>, though, so posterior regenerating processes are needed. Here, materials that allow for a continuous separation without regeneration interruption steps would be better adequate.

Related to the previous, 2D porous membranes are gaining some popularity for selective diffusion processes. For instance, promising results have been achieved in studies on graphene nanostructures [6] and reduced graphene oxides [7]. Another carbon allotrope that has shown good results are graphynes [8], 2D carbon-based structures with C atoms displaying *sp* and *sp*<sup>2</sup> hybridizations, e.g., displaying C *sp*<sup>2</sup> nodes linked together by acetylenic bonds between them, this is, through C atoms with *sp* hybridization. Some theoretical studies on graphynes pointed out their superior charge transportation compared to graphene [8–10], and proposed synthetic routes to achieve them [11].

Grazynes are a subtype of graphynes, whose structural, electronic, and elastic properties have been studied by density functional theory (DFT) [12]. Grazynes are composed by graphene stripes in which C atoms display *sp*<sup>2</sup> hybridization, linked by acetylenic linkages, where C atoms have *sp* hybridization, see Fig. 1. Such structures have been proposed to display a peculiar new type of electronic current transportation across acetylenic neighbors [13]. Moreover, grazynes structure can be modified in different ways, either widening the width of the graphene stripes, enlarging the acetylenic bonds, or creating vacancies in such bonds.

This high tunability allows the size of the pores present in the structure to be modified at will and profited in turn to maximize the chemical resolution of gases; this is, finding pore sizes that allow some molecules to pass across the membrane while others do not, and, by that, controlling the diffusion selectivity. This principle is applicable to biogas upgrading, separating CH<sub>4</sub> from CO<sub>2</sub>, but it could be used to foster/inhibit the pass of other molecules, such as hydrogen, nitrogen carriers, or nitrogen dioxide exhaust gas contaminant, to name a few.

The present work aims at computationally studying biogas upgrading on grazyne structures in a holistic, multiscale fashion, regarding thermodynamic, kinetic, and dynamic aspects, estimating the diffusion rates and selectivity of CO<sub>2</sub> and CH<sub>4</sub> on a set of grazyne structures having

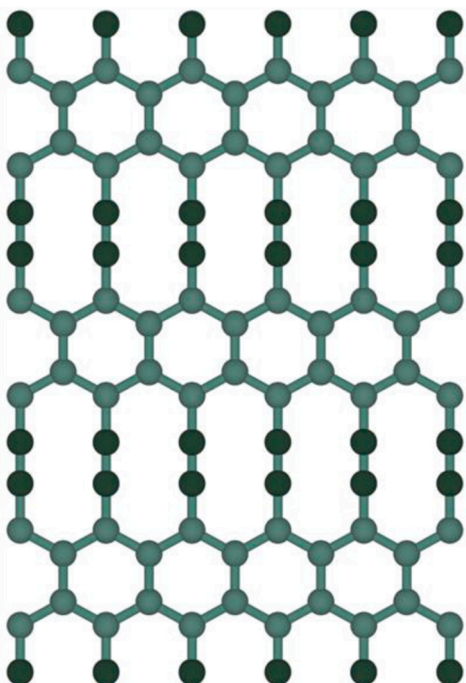


Fig. 1. Top view of [1],[1]-grazyne. Dark and light green spheres correspond to *sp*- and *sp*<sup>2</sup>- C atoms, respectively.

different permeability, with the ultimate goal of assessing whether certain nano-engineered grazyne structures would be suited materials for biogas upgrading applications.

## 2. Computational methods

### 2.1. Density functional calculations

Theoretical simulations on the CO<sub>2</sub> and CH<sub>4</sub> diffusion process have been carried out using periodic DFT based calculations on the grazyne structures shown in Fig. 2, through the Vienna *ab initio* simulation package (VASP) [14]. The core electron density was described by the projector augmented wave (PAW) method of Blöchl [15], while the valence electron density was built as a function of a plane-wave basis set of 415 eV of kinetic energy cutoff. To account for exchange-correlation (xc) effects, the Perdew-Burke-Ernzerhof (PBE) xc functional was used [16], including Grimme's D3 description of dispersive forces (PBE-D3) [17]. Both CO<sub>2</sub> and CH<sub>4</sub> isolated molecules were fully optimized at  $\Gamma$  k-point in a large, cubic unit cell of  $10 \times 10 \times 10 \text{ \AA}^3$ , with an electronic convergence threshold of  $10^{-6}$  eV and an ionic convergence threshold of  $10^{-5}$  eV.

Different grazyne structures have been regarded in the study, departing from the smallest [1],[1]-grazyne, shown in Fig. 1, built from a graphene stripe of one benzene unit wide and with one double bond for the acetylenic linkages knitting the graphene stripes, which explain the two [1] in the notation, as proposed in Ref. [12]. Such a grazyne would be, *a priori*, excessively atomically packed, not allowing the diffusion of neither CO<sub>2</sub> nor CH<sub>4</sub>, and selected as a possible impermeable membrane. Other than this, a pore has been nano-engineered in [1],[1,2]{0,1}-grazyne, see Fig. 2a, maintaining the graphene stripe width, yet enlarging the acetylenic linkages up to two double bonds—there the [2] in the notation—, and having an acetylenic link vacancy in every second case—there the {1} in the notation meaning that there is one empty space in between consecutive acetylenic linkages—. This grazyne was selected since could be a potential semi-permeable membrane, featuring different diffusion energy barriers for CO<sub>2</sub> and CH<sub>4</sub>.

Finally, two potentially permeable membranes have been explored, the [1],[2]{2}-grazyne and the [1],[2]{(00),2}-grazyne, shown in Figs. 2b and 2c, respectively. As before, the smallest graphene stripe is maintained, as well as the longitude of the acetylenic linkage, but the pore size is increased by having two consecutive acetylenic vacancies. The main difference in between the two materials is the presence of isolated acetylenic linkages in [1],[2]{2}-grazyne, but having two neighboring acetylenic linkages followed by two vacancies in the [1],[2]{(00),2}-grazyne case—there the {(00),2} notation—.

For the aforementioned selected grazyne membranes,  $c(1 \times 1)$  periodic supercells were built and fully optimized, with a vacuum space of  $10 \text{ \AA}$  added up and down of the 2D sheet, perpendicularly to the grazyne surface, in order to avoid interactions between periodically repeated grazyne layers. For such structures, an optimal Monkhorst-Pack k-point grid of  $10 \times 10 \times 1$  was employed, guaranteeing to acquire energies converged below the chemical accuracy of  $1 \text{ kcal mol}^{-1}$ —ca.  $0.04 \text{ eV}$ —, as tested employing larger k-point grids and basis set sizes. The same k-point grid has been used for the larger  $c(2 \times 2)$  supercell. Note that, when creating defective sites on the structures, dangling covalent bonds have been capped with hydrogen atoms, as customary, as it can be seen in Fig. 2. Table 1 shows the optimized cell parameters for each grazyne model indicating that enlarging the acetylenic pore increases the value of *a* and *b* cell parameters.

The DFT optimizations needed to gain the diffusion energy profiles have been carried out by relaxing the entire grazyne surface except for one carbon atom, kept frozen in the three directions of the space, to avoid the overall material drifting, and ensuring that forces acting on atoms were below  $0.01 \text{ eV \AA}^{-1}$ . Once minima and transition states have been found, the geometries were further optimized letting relax all atoms, *i.e.*, at this point no C atom was kept fixed. The adsorption of CO<sub>2</sub>

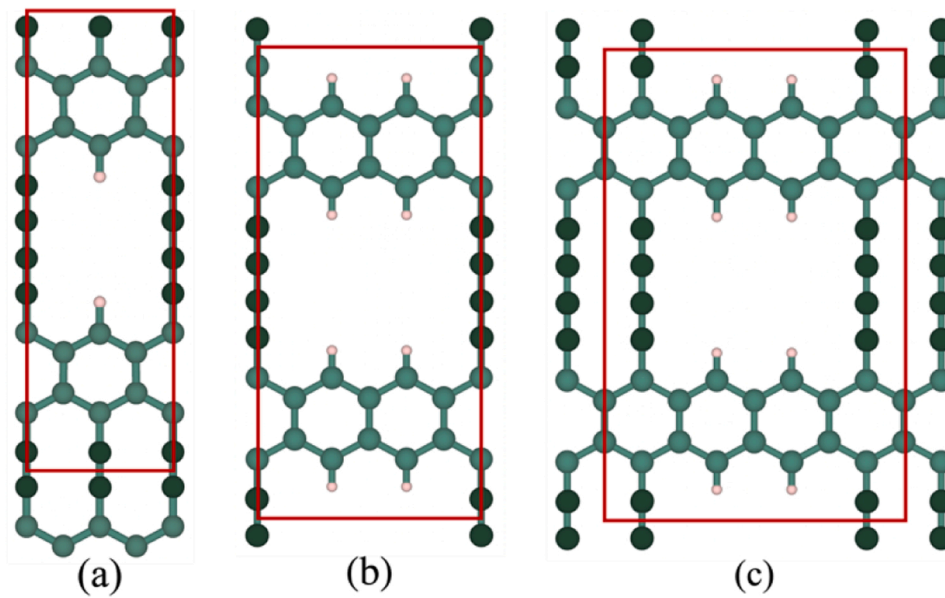


**Fig. 2.** Top view of (a) [1],[1,2]{0,1}-grazyne, (b) [1],[2]{2}-grazyne, and (c) [1],[2]{(00),2}-grazyne. White spheres denote H atoms, while the rest of color coding is as in Fig. 1.

**Table 1**

In plane cell parameters,  $a$  and  $b$ , for each studied grazyne.

Grazyne <sup>a</sup>	$a/\text{Å}$	$b/\text{Å}$
[1],[1]	5.106	13.624
[1],[1,2]{0,1}	5.127	16.142
[1],[2]{2}	7.659	18.573
[1],[2]{(00),2}	10.212	18.573

<sup>a</sup> Note that  $a$  and  $b$  directions are orthogonal.

and CH<sub>4</sub> on the named models was done likewise.

The location of the diffusion transition states through the material pores was carried out in a point-wise fashion. To this end, the CO<sub>2</sub> or CH<sub>4</sub> molecules center of mass was aligned with the pore geometric center, and placed distant from the pore center, at  $\sim 5$  Å. For such an initial geometry, different molecular conformations were considered. Thus, CO<sub>2</sub> was placed perpendicular and parallel to the grazyne plane, *albeit* for CH<sub>4</sub> only the geometry with a hydrogen pointing towards the grazyne has been considered, the lowest energetic approach to the membrane according to test calculations. During the optimizations, CO<sub>2</sub> and CH<sub>4</sub> carbon atoms along with the most distant membrane C atom to the analyzed pore were kept frozen whereas the rest of atoms were allowed to fully relax. After the optimization, the molecule is successively approached to the pore, until the transition state is reached. Minima and transition states are then characterized by frequency analysis, through building and diagonalizing the Hessian matrix, constructed by finite atomic displacements of 0.03 Å length, finding none or one imaginary frequency for minima and transition states, respectively.

The molecular adsorption energies,  $E_{ads}^i$ , for  $i$ -species CO<sub>2</sub> and CH<sub>4</sub> on the grazyne models were calculated as,

$$E_{ads}^i = E_{S/i} - E_S - E_i, \quad (1)$$

where  $E_{S/i}$  is the energy with the adsorbed molecule on the grazyne substrate,  $E_S$  represents the grazyne substrate energy, and  $E_i$  is the energy of the molecule in its ground state. Once the transition state for the explored molecule trespassing the membrane and the minimum of adsorption on the surface were obtained, the diffusion energy barrier across the membrane,  $E_b^i$ , has been obtained as,

$$E_b^i = E_{TS,i} - E_{S/i}, \quad (2)$$

where  $E_{TS,i}$  is the transition state energy for  $i$ -species. Both  $E_{ads}^i$  and  $E_b^i$  terms have been corrected by applying the zero-point energy (ZPE) correction, adding the  $E_{ZPE}$  according to,

$$E_{ZPE} = \frac{1}{2} \sum_i^{NMV} \hbar \nu_i, \quad (3)$$

where  $\hbar$  is the Planck constant, and  $\nu_i$  each of the normal modes of vibration (NMV). Note that the transition state imaginary frequency is not considered in the ZPE correction. Aside, by using transition state theory (TST), and once frequency calculations have been made, it is possible to estimate the diffusion selectivity of CO<sub>2</sub> over CH<sub>4</sub> with the following expression,

$$S_{CO_2/CH_4} = \frac{r_{CO_2}}{r_{CH_4}} = \frac{e^{-E_b^{CO_2}/k_B T}}{e^{-E_b^{CH_4}/k_B T}}, \quad (4)$$

where  $r_{CO_2}$  and  $r_{CH_4}$  are the diffusion rates for CO<sub>2</sub> and CH<sub>4</sub>, respectively,  $k_B$  is the Boltzmann constant,  $T$  the working temperature, and  $E_b^{CO_2}$  and  $E_b^{CH_4}$  the diffusion energy barriers for CO<sub>2</sub> and CH<sub>4</sub>, respectively. As can be seen in Eq. (4), it is mandatory to have estimates of the diffusion rate constants for both molecules in order to calculate the selectivity. Diffusion rates are estimated by TST through the general expression for  $i$ -species,

$$r_i = \frac{k_B T}{h} \frac{q_{vib,i}^\ddagger}{q_{vib,i}^{ads}} e^{-\frac{E_b^i}{k_B T}}, \quad (5)$$

where  $q_{vib,i}^\ddagger$  and  $q_{vib,i}^{ads}$  terms stand for the vibrational partition function for the transition state and for the adsorbed minimum geometry, respectively (*i.e.*, the CO<sub>2</sub> or CH<sub>4</sub> adsorbed on one side of the grazyne pore, see below). Given the adsorbed geometry for CO<sub>2</sub> and CH<sub>4</sub>, only the vibrational partition function is needed because rotational and translational modes become frustrated by the substrate presence and the formed bond in the adsorption. Thus,  $q_{vib,i}$  can be calculated as,

$$q_{vib,i} = \prod_j^{NMV} \frac{1}{1 - e^{-\frac{\hbar \nu_j}{k_B T}}}, \quad (6)$$

where the frequencies run over all NMV in the case of minima. For the transition state vibrational partition function,  $q_{vib,i}^\ddagger$ , the product runs

over all the vibrational frequencies except the imaginary one.

By this analysis, we investigated on the grazyne structures drawn in Fig. 2, the adsorption thermodynamics, (*i.e.*, whether CO<sub>2</sub> and CH<sub>4</sub> can get physisorbed or chemisorbed), the kinetics, through the magnitude of the diffusion energy barriers, the rates of diffusion, and the selectivity of CO<sub>2</sub> diffusion over CH<sub>4</sub>, as a function of temperature. Finally, with the above data it is also possible to calculate the desorption rates,  $r_{des,i}$ , of the  $i$ -adsorbate for the grazyne structures. To do so, a late transition state is assumed within TST, and so, the desorption rate can be expressed as follows,

$$r_{des,i} = S_{des,i} \nu_{des,i} e^{-\frac{E_i}{k_B T}}, \quad (7)$$

where  $\nu_{des,i}$  is defined as,

$$\nu_{des,i} = \frac{k_B T}{h} \frac{q_{trans,i} q_{rot,i} q_{vib,i}}{q_{vib,i}^{ads}}, \quad (8)$$

being  $q_{trans,i}$ ,  $q_{rot,i}$ , and  $q_{vib,i}$  the translational, rotational, and vibrational partition functions for  $i$ -species, CO<sub>2</sub> and CH<sub>4</sub> molecules, in gas phase. For such expressions we refer to literature [18]. The  $q_{vib,i}^{ads}$  is the vibrational partition function of the adsorbed molecule—where rotations and translations are frustrated by the interaction with the grazyne substrate, and so, converted de facto into vibrations—. Finally,  $S_{des,i}$  corresponds to the desorption coefficient, defined in the range [0,1], implying the probability that a molecule would escape from the surface when having the necessary energy. In the present study, we have considered desorption coefficients as unity for both species.

Aside, it is also possible to calculate the adsorption rate with the following expression,

$$r_{ads,i} = \frac{S_{0,i} p_i A_i}{\sqrt{2\pi m_i k_B T}}, \quad (9)$$

where  $m_i$  is the molecular mass of CO<sub>2</sub> or CH<sub>4</sub>,  $A_i$  the adsorption area associated to each species, and  $S_{0,i}$  the sticking coefficient, *i.e.*, the probability that a molecule arriving at the surface will remain adsorbed, and  $p_i$  corresponds to the partial pressure of  $i$ -species. When calculating  $r_{ads,i}$ , a conservative  $S_{0,i}$  value of 0.2 has been used for both CO<sub>2</sub> and CH<sub>4</sub>, verified to be a suited value for CO<sub>2</sub> capture and biogas upgrading [5, 18]. Finally, as previously mentioned, there are different aspects that have not been regarded in the DFT calculations yet may be key in order to get more representative results. To complement DFT calculations, molecular dynamics simulations have been carried out, where it has been possible to consider different aspects such as the pressure of the gas stream, the working temperature or even interpret the different interactions that occur between the simulated gas molecules such as those that are produced with the porous material. Given the methodologically differences between DFT and MD runs, the latter are detailed in the next section for better clarity.

## 2.2. Molecular dynamics

To investigate the dynamics of the CO<sub>2</sub> and CH<sub>4</sub> diffusion across the grazyne membrane, several classical MD simulations have been carried out using the LAMMPS package [19]. All simulations consisted of a grazyne membrane model and a mixture of CO<sub>2</sub> and CH<sub>4</sub> molecules at 50 % (v/v). As before, periodic boundary conditions were applied over  $c$  ( $8 \times 8$ ) supercell structures constructed from the basic unit cell. In order to avoid the membrane translation during the simulation, a carbon atom was fixed in such a way that the drift was eluded. All simulations have been carried out at a working temperature of 300 K. The effect of pressure on the diffusion process of the two molecules has been considered, increasing and decreasing the pressure of the gas mixture.

The initial configurations were built by distributing 128 total molecules of CO<sub>2</sub> and CH<sub>4</sub> on top of the grazyne surface. From this point on, a process of thermalization at 300 K of the gas mixture was performed.

In order to carry out this process, a wall has been placed just above the grazyne mesh and another wall ranging from 20 to 60 Å above it, depending on the mixture pressure, so that the gas mixture remains between the two walls, see Fig. 3. This process ran for  $10^6$  steps, with a time step of 0.1 fs, for a total time of 100 ps. Once the mixture is thermalized, the lower wall has been removed and the simulation of the diffusion process was carried out during  $4 \cdot 10^6$  steps at the same time-step of 0.1 fs, for a total time of 400 ps. In this part of the simulation two walls have been also used. A wall has been placed at the lower edge of the simulation box and another upper wall that is the same one that has been used in the thermalization process. This upper wall allows us to vary the pressure of the system depending on the height at which it is placed; the higher up the  $z$  axis, the more volume,  $V$ , and so, the less pressure,  $p$ , for a given temperature,  $T$ , and *vice versa*. No interactions were assumed between walls and molecules and membrane.

The total energy of the system is described by a sum of bonded and non-bonded pairwise interactions. Bonds and angles for CH<sub>4</sub> and CO<sub>2</sub> species are represented by harmonic potentials through the general equations,

$$V_{bonded}(r_{ij}) = \frac{1}{2} k_r (r_{ij} - r_{eq})^2, \quad (10)$$

$$V_{bonded}(\theta_{ij}) = \frac{1}{2} k_\theta (\theta_{ij} - \theta_{eq})^2, \quad (11)$$

where  $k_r$ ,  $k_\theta$ ,  $r_{eq}$ , and  $\theta_{eq}$  are parameters set to define the interaction between atoms, being the former the strength constants for bonding and bending, and the latter the equilibrium values for bond distance and angle, respectively. The used parameters are shown in Table 2. The AIREBO force field [20] has been used to describe the behavior of the grazyne membrane and methane. Finally, the CO<sub>2</sub> molecules have been described by a Lennard-Jones 12-6 potential [21]. For non-bonded atoms the unlike pair parameters were calculated from the Lorentz-Berthelot combination rules (*i.e.*,  $\epsilon_{ij} = \sqrt{\epsilon_i \epsilon_j}$  and  $\sigma_{ij} = (\sigma_i + \sigma_j)/2$ ). Moreover, electrostatic interactions have been also considered through the Coulomb interaction term,

$$V_{non-bonded}(r_{ij}) = \frac{q_i q_j}{4\pi \epsilon_0 r_{ij}} + 4\epsilon_{ij} \left( \left( \frac{\sigma_{ij}}{r_{ij}} \right)^{12} - \left( \frac{\sigma_{ij}}{r_{ij}} \right)^6 \right), \quad (12)$$

where  $\epsilon_0$  is the vacuum permittivity,  $\epsilon_{ij}$  and  $\sigma_{ij}$  are the Lennard-Jones parameters,  $r_{ij}$  the distance between pairs, and  $q_i$ ,  $q_j$  the partial atomic charges of  $i$ - and  $j$ -species, see Table 3.

Apart from checking how the adsorbates interact within the membrane in the simulations, one of the main goals of this part is to calculate the membrane selectivity for each molecule. To do this, a FORTRAN code has been created that reads the trajectory file generated by LAMMPS and counts how many CO<sub>2</sub> and CH<sub>4</sub> molecules pass across the grazyne at each time step, freely available at GitHub [22]. Furthermore, the gas molecular flow is normally used to characterize the membrane permeability,  $P_i$ , which is defined as [23],

$$P_i = \frac{N_i}{S \cdot t}, \quad (13)$$

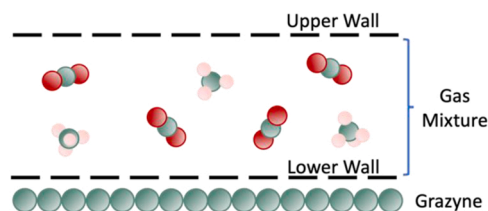


Fig. 3. Visual scheme of the thermalization process. The black dashed lines represent the placed walls that allow gas thermalization without interaction with membrane. Oxygen atoms are represented by red spheres. The rest of color coding as in Fig. 2.

**Table 2**

Bond and angle coefficients used in the MD simulations.

Molecule	$r_{eq}/\text{\AA}$	$k_r/eV\text{\AA}^{-2}$	$\theta_{eq}/^\circ$	$k_\theta/eV\text{ deg}^{-2}$
CH <sub>4</sub>	1.09	14.74	107.8	1.43
CO <sub>2</sub>	1.16	6.16	180	6.45

**Table 3**

Non-bonded parameters used in MD simulations.

Atom	$q/e$	$\epsilon_r/eV$	$\sigma_i/\text{\AA}$
Hydrogen (in CH <sub>4</sub> )	0.06	airebo	airebo
Carbon (in CH <sub>4</sub> )	-0.24	airebo	airebo
Carbon (in CO <sub>2</sub> )	0.65	0.00242	2.757
Oxygen	-0.33	0.00694	3.033

where  $N_i$  are the moles of permeated gas molecules through the membrane in both directions,  $S$  corresponds to the area of the membrane, and  $t$  is the simulation time.

### 3. Results and discussion

#### 3.1. CO<sub>2</sub> diffusion

In the following, DFT calculations of CO<sub>2</sub> and CH<sub>4</sub> have been carried out separately for both molecules, this is, a single molecule has been considered in the grazyne pore, with no cases with simultaneously two molecules on it, since the latter would be highly unlikely situations. In addition, when two molecules would be in the same pore at the same time, they would rather repel each other, complicating diffusion through the grazyne, and, on the other hand, their simultaneous diffusion would be impeded by their volume. Passage of CO<sub>2</sub> molecules across grazyne membranes has been considered over two possible molecular orientations, with the molecular axis being either perpendicular or parallel to the grazyne plane. Both orientations were considered for [1],[2]{2}-grazyne and [1],[2]{(00),2}-grazyne structures (Figs. 2b and 2c) whereas for [1],[1]-grazyne and [1],[1,2]{0,1}-grazyne (Figs. 1 and 2a) the parallel orientation was not considered since, as the grazyne pore is not large enough, the repulsion between substrate and molecules is expected to be very high. The obtained adsorption energies,  $E_{ads}^i$ , are listed in Table 4 together with the diffusion energy barriers,  $E_b^i$ .

In order to study a given diffusion process, it must be borne in mind that barrier energies lower than  $\sim 1$  eV would be preferable for this process to happen in a significant amount. Besides, it would be desirable that molecules would feature small adsorption energies, ideally belonging to physisorption processes, rather than larger values proper to chemisorption, since, in the latter case, that would imply that the material would act as sweep molecular material, rather than acting as a filtering membrane, although molecular and/or trapping membranes can be useful, e.g., in cleaning or water desalination processes [24,25]. By inspecting Table 4, it is clear that the adsorption energies for CO<sub>2</sub> are quite small, ranging from  $-0.08$  eV to  $-0.19$  eV in defective grazyne models. Moreover, perpendicular and parallel orientations of CO<sub>2</sub> correspond to physisorption processes being the perpendicular

**Table 4**Adsorption and diffusion energy barriers for CO<sub>2</sub> on different grazyne structures at perpendicular or parallel orientations. All values are given in eV.

Grazyne	Perpendicular		Parallel	
	$E_{ads}^{CO_2}$	$E_b^{CO_2}$	$E_{ads}^{CO_2}$	$E_b^{CO_2}$
[1],[1]	0.01	11.13	—	—
[1],[1,2]{0,1}	-0.08	0.62	—	—
[1],[2]{2}	-0.19	0.13	-0.13	0.49
[1],[2]{(00),2}	-0.19	0.13	-0.12	0.86

adsorption preferred by 0.06 eV and 0.07 eV in [1],[2]{2}- and [1],[2]{(00),2}-grazyne, respectively.

In addition, the diffusion across the most packed grazyne, [1],[1]-grazyne, is prohibitive, with an  $E_b^{CO_2}$  of more than 11 eV. Other than this, the rest of the values are all under 1 eV, so, taking this as an indicator, the CO<sub>2</sub> could diffuse across all the structures, although at different rates. At present, it seems as parallel conformations on [1],[2]{2}- and [1],[2]{(00),2}-grazyne structures display significant barriers of 0.49 eV and 0.86 eV, respectively; of the same order of the perpendicular diffusion on [1],[1,2]{0,1}-grazyne, with an  $E_b^{CO_2}$  of 0.62 eV. On the other hand, perpendicular diffusion across [1],[2]{2}- and [1],[2]{(00),2}-grazyne have a smaller barrier of only 0.13 eV. Thus, the diffusion of CO<sub>2</sub> molecules perpendicularly to the grazyne plane is much more favored than the parallel orientation. In the case of parallel orientation, CO<sub>2</sub> only can pass across [1],[2]{2}- and [1],[2]{(00),2}-grazyne structures although the highest barrier is obtained for the latter one (i.e.,  $E_b^{CO_2} = 0.86$  eV). Aside, notice that, for such semi-permeable grazyne, the stronger the physisorption, the smaller the diffusion barrier,  $E_b^{CO_2}$ . Considering the values listed in Table 4, the diffusion coordinate for each studied system is shown in Fig. 4, where it is evidenced that perpendicular orientations provide lower energy profiles than parallel orientations.

Apart from the diffusion energy profiles, during the mentioned optimizations it has been observed that, depending on the grazyne structure, different deformations occur. For example, in the transition state associated to the CO<sub>2</sub> diffusion across the [1],[2]{(00),2}-grazyne, the acetylenic bonds bulge towards the adsorbate, in an attractive fashion, see Fig. 5. As this type of grazyne contains a larger pore, the CO<sub>2</sub> molecule does have enough space to cross the membrane, so an attractive interaction between the carbons of the acetylenic stripes and the CO<sub>2</sub> molecule may happen. This bulging is actually observed for both orientations of CO<sub>2</sub>.

The deformation observed in [1],[2]{(00),2}-grazyne does not occur in the [1],[2]{2}-grazyne membrane because the two consecutive acetylenic strings present in the former cause the adsorption centers (i.e., center of the pore) to be further away from each other than in the [1],[2]{2}-grazyne where the single acetylenic string interacts simultaneously with the two CO<sub>2</sub> molecules avoiding any deformation of the structure.

Essentially, the [1],[2]{(00),2}-grazyne structure decreases the number of possible and simultaneous interactions with the acetylenic parts and gives them more freedom to conform a more suitable geometry for the CO<sub>2</sub> adsorptions and diffusion. Although this fact has no significant impact for neither  $E_{ads}^{CO_2}$  nor  $E_b^{CO_2}$  for perpendicular CO<sub>2</sub> orientations, see Table 4, it does for parallel orientations, especially on the transition states, with a difference of almost 0.4 eV in  $E_b^{CO_2}$ . Finally, no deformation was observed in the [1],[1,2]{0,1}-grazyne.

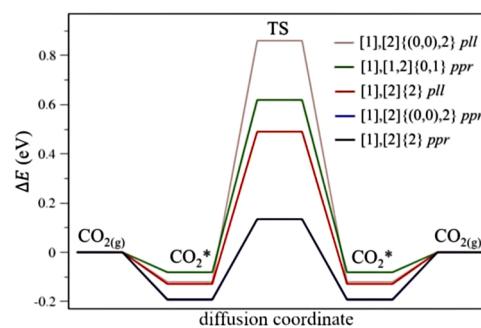


**Fig. 4.** Energy profiles for the perpendicular (ppr) and parallel (pll) diffusion coordinate of CO<sub>2</sub> across different grazyne structures. TS represents the transition state and CO<sub>2</sub>\* the adsorbed state.

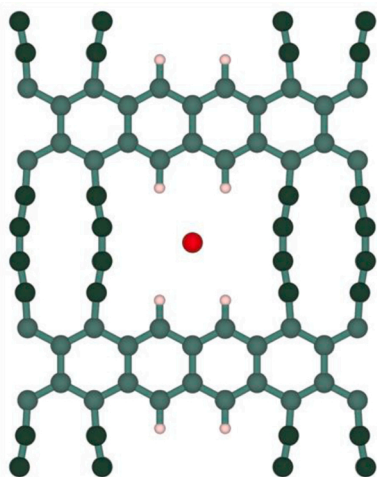


Fig. 5. Top view of [1],[2]{(00),2}-grazylene transition state for CO<sub>2</sub> diffusion across the pore. Color coding as in Fig. 3.

### 3.2. Coverage

Having observed that the [1],[1,2]{0,1}-grazylene is the one with a higher diffusion energy barrier for CO<sub>2</sub>, the coverage effect has been also analyzed. Thus, the coverage,  $\theta$ , has been set at 50 % (occupying half of the pores of the cell) and at 100 % (occupying all the pores of the cell), as shown in Fig. 6. The results at full coverage are those shown in Table 4 and the comparison with half coverage is shown in Table 5. It is worth noting that by decreasing the coverage, the  $E_{ads}^{CO_2}$  decreases by 0.05 eV, probably due to favorable lateral interactions at full  $\theta$ , but, on the other hand, the  $E_b^{CO_2}$  value decreases as well by ca. 0.3 eV. This difference can be explained from the deformations observed in Fig. 7. The fact of having half coverage allows the grazylene to widen the acetylenic links, and by that, the pore size, in order to offer CO<sub>2</sub> more space to diffuse through, having less repulsion in between the molecule and the acetylenic linkages. This deformation is also observed in the optimization of the adsorbed CO<sub>2</sub> but in a much lesser extent. As expected, the adsorbed minimum is located ca. 2 Å away from the grazylene pore center, so the steric repulsion is much attenuated. Apart from this, no membrane deformations out of grazylene plane have been observed.

At full coverage, all pores are simultaneously occupied by CO<sub>2</sub> molecules, so the bulging effect cannot happen. Still, one has to keep in mind that the simultaneous trespassing of two CO<sub>2</sub> molecules on vicinal pores is probably a rare event, something that could be inspected by the MD simulations.

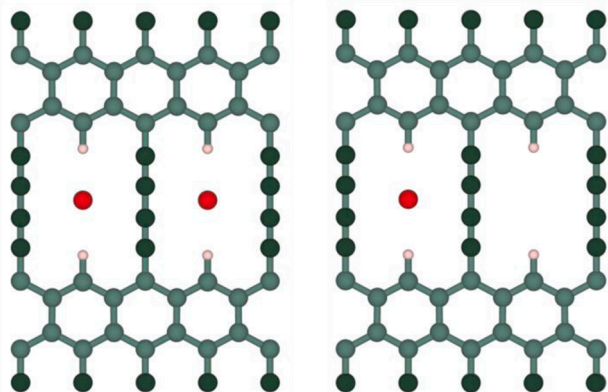


Fig. 6. Top view of [1],[1,2]{0,1}-grazylene with  $\theta = 100\%$  (left) and  $\theta = 50\%$  (right). Color coding as in Fig. 3.

Table 5

Adsorption and diffusion energy barriers for CO<sub>2</sub> on [1],[1,2]{0,1}-grazylene model at different coverages.

$\theta$ (%)	$E_{ads}^{CO_2}$ /eV	$E_b^{CO_2}$ /eV
50	-0.03	0.35
100	-0.08	0.62

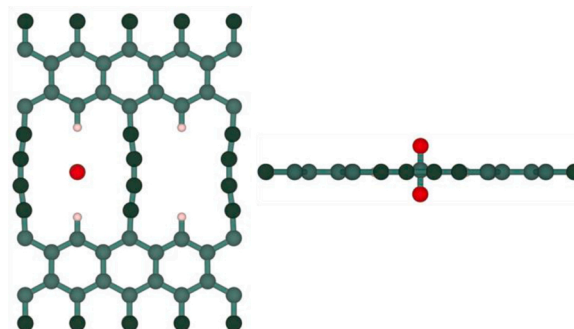


Fig. 7. Top (left) and side (right) view of [1],[1,2]{0,1}-grazylene at the transition state for the CO<sub>2</sub> diffusion across the pore. Color coding as in Fig. 3.

### 3.3. CH<sub>4</sub> diffusion

The CH<sub>4</sub> adsorption and diffusion has been evaluated on the grazylene models in a likewise fashion as done for CO<sub>2</sub> although only one type of orientation has been considered for methane, that pointing one hydrogen atom down towards the grazylene membrane. Table 6 lists the adsorption and diffusion energies obtained. Again, grazylens with a higher pore size featured larger  $E_{ads}^{CH_4}$  values of  $-0.17$  eV, belonging to a physisorption process. A similar situation is found for [1],[1,2]{0,1}-grazylene compound, with an  $E_{ads}^{CH_4}$  of  $-0.12$  eV. However, the main differences between the grazylene structures are in the diffusion energy barriers. The [1],[1,2]{0,1}-grazylene compound displays a very large  $E_b^{CH_4}$  of 2.36 eV, which represents a very high value for an energy barrier, to the point of safely claiming that methane would not be able to pass through this grazylene, being impermeable to CH<sub>4</sub>. The same happens for [1],[1]-grazylene, where, despite the  $E_{ads}$  of  $-0.11$  eV, the trespassing yielded to very high energies where the grazylene layer became broken. For the two remaining grazylens, the  $E_b^{CH_4}$  values obtained are 0.22 eV and 0.31 eV for [1],[2]{2}- and [1],[2]{(00),2}-grazylene, respectively, which are suited for CH<sub>4</sub> diffusion. These values are between 0.09 and 0.18 eV higher than for CO<sub>2</sub>, but low enough to expect methane diffusion across these structures.

In addition, considering the results obtained in the previous section for CO<sub>2</sub>, a lower coverage of methane (50 %), has been considered for [1],[1,2]{0,1}-grazylene obtaining a 15 % decrease in the diffusion barrier. As happened with CO<sub>2</sub>, deformations are observed for CH<sub>4</sub> on the studied grazylens, being of the same type as those seen for CO<sub>2</sub> diffusion, but much more accentuated. Particularly, for the [1],[1,2]{0,1}-grazylene

Table 6

Adsorption and diffusion energy barriers of CH<sub>4</sub> on different grazylene structures at full coverage.

Grazylene	$E_{ads}^{CH_4}$ /eV	$E_b^{CH_4}$ /eV
[1],[1]	-0.11	— <sup>a</sup>
[1],[1,2]{0,1}	-0.12	2.36
[1],[2]{2}	-0.17	0.22
[1],[2]{(00),2}	-0.17	0.31

<sup>a</sup> Note that the compound [1],[1]-grazylene has no value for  $E_b$  because the structure was broken due to the high repulsions.

shown in Fig. 8, the bulging of the acetylenic bonds is more pronounced. Deformations were observed for both the transition state and the adsorbed state, as well for the [1],[2]{(00),2}-grazyne. Finally, no deformations were observed in the [1],[2]{2}-grazyne.

### 3.4. Rate constants

Once it has been determined that [1],[1,2]{0,1}-, [1],[2]{2}-, and [1],[2]{(00),2}-grazyne seem to be capable of filtering CO<sub>2</sub> and, to a lesser extent, CH<sub>4</sub>, the rate constants for trespassing the membrane at different temperatures have been calculated through Eq. (5) after ZPE correction of diffusion energy barriers in accordance with Eq. (3). The obtained rates for the diffusion of CO<sub>2</sub> placed perpendicular to the grayzine sheet and CH<sub>4</sub> placed with a hydrogen pointing towards the grayzine plane are shown in Fig. 9.

In it, it is possible to see that CO<sub>2</sub> has systematically larger rates compared to CH<sub>4</sub>. It is clear as well that as the temperature increases, the rate constants also increase. Finally, it is worth noting that large diffusion rates would be desirable in the screened temperature range of 100–500 K, for instance, with  $r_i$  being above  $1 \text{ s}^{-1}$ . That is achieved for both CO<sub>2</sub> and CH<sub>4</sub> on [1],[2]{2}-grazyne semi-permeable membrane, with large pore sizes, and similarly in the case of CO<sub>2</sub> on [1],[2]{(00),2}-grazyne structure. However, on this latter membrane CH<sub>4</sub> achieves  $r_i$  values above  $1 \text{ s}^{-1}$  only at temperatures above ca. 200 K. Finally, the [1],[1,2]{0,1}-grazyne model, showing larger diffusion barriers (Table 2 and Table 5) features very low  $r$  values, which can be above  $1 \text{ s}^{-1}$  for CO<sub>2</sub> above ~200 K, but within the range  $10^{-60} \text{ s}^{-1}$  (100 K) to  $10^{-4} \text{ s}^{-1}$  (500 K) for CH<sub>4</sub>. Overall, clearly the nano-engineering of double vacancy pores allows for a more rapid diffusion of CO<sub>2</sub>, but at the expense of making CH<sub>4</sub> diffusion also possible, which may have an impact in the overall membrane selectivity.

### 3.5. Selectivity

The selectivity of CO<sub>2</sub> diffusion across the grayzine membrane compared to CH<sub>4</sub> can be calculated through Eq. (13). After analyzing the obtained energy values for both molecules, it seems that perpendicular CO<sub>2</sub> will be able to pass across the membranes through the largest acetylene pores while methane featuring higher energy barriers, could not being able to cross, e.g., in [1],[1,2]{0,1}-grazyne. To better assess this, the calculated selectivity values are shown in Fig. 10 as a function of the temperature within the range 100–500 K and considering the same casuistry exposed in Fig. 9.

It is clear from Fig. 10 that the selectivity decreases with temperature for the three grayzine membranes, in full accordance with the rates shown in Fig. 9. The larger the temperature, the more similar are the CO<sub>2</sub> and CH<sub>4</sub> rates, and the closer is the selectivity ratio to one. This

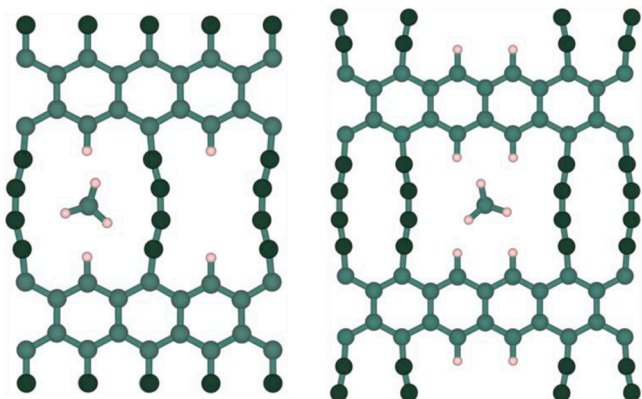


Fig. 8. Top view of [1],[1,2]{0,1} (left) and [1],[2]{(00),2} (right) compounds at transition state of CH<sub>4</sub> diffusion across the pore. Color code as in Fig. 3.

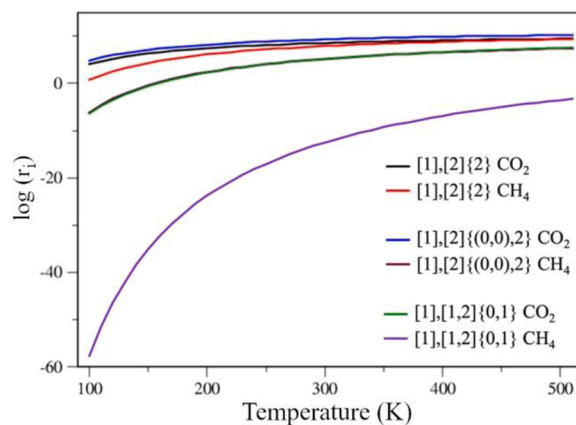


Fig. 9. Rate constants estimates,  $r_i$ , for perpendicular CO<sub>2</sub> and CH<sub>4</sub> diffusion through the different grayzine membranes as a function of temperature.

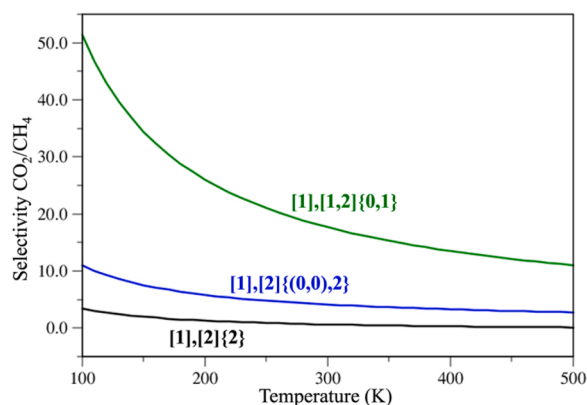


Fig. 10. CO<sub>2</sub> selectivity over CH<sub>4</sub> for the studied grayzines as a function of temperature.

would ask for working at low temperatures to attain better selectivity values, but one has to keep in mind that, in such situations, the rates of diffusion would be smaller as well, compromising the biogas upgrading production rate. Inspecting the particular cases, the [1],[1,2]{0,1}-grazyne has a high CO<sub>2</sub> selectivity over CH<sub>4</sub> at room temperature, of nearly 17, while, for the rest of grayzines, the selectivity of CO<sub>2</sub> is much lower, below five. Thus, it appears that [1],[1,2]{0,1}-grazyne is the best biogas upgrading membrane candidate, even if having smaller diffusion CO<sub>2</sub> rates than the other two grayzines (Fig. 9). Actually, for the other two grayzine semi-permeable structures, the CO<sub>2</sub> rates can be three to four orders of magnitude higher than those for CH<sub>4</sub>, but at the expense of being more permeable to CH<sub>4</sub> as well, and therefore, less selective. In this sense, considering both rates and selectivity, the [1],[2]{(00),2}-grazyne exhibits the better compromise between selectivity and rate of filtering, followed by the [1],[2]{2}-grazyne.

### 3.6. Kinetic phase diagrams

Even though from the above discussion and analysis the semi-permeable grayzines models could be suited for biogas upgrading, one should also rule out the possible adsorption of CO<sub>2</sub> or CH<sub>4</sub> on them, a situation that would make them suited sweep materials, but which is not optimal for a continuous working process, as above stated. Thus, ideally, neither CO<sub>2</sub> nor CH<sub>4</sub> should adsorb on the grayzine models at working conditions. This is evaluated here by making use of the so-called kinetic phase diagrams [26], gained from the calculated desorption and adsorption rates,  $r_{des,i}$  and  $r_{ads,i}$ , for both CO<sub>2</sub> and CH<sub>4</sub> on the grayzine models. Briefly, both rates are gained as a function of the gas pressure

and temperature, following Eqs. (7) and (9), respectively. The equilibrium situation is reached when both rates become equal (i.e.,  $r_{ads,i} = r_{des,i}$  for the same  $i$ -species). This has been done for different  $p$  and  $T$  conditions, dividing the  $p/T$  space in two regions, one dominated by the adsorption, where the molecules would tend to accumulate on the material surface, and one dominated by the desorption, where the surface would remain essentially clean.

This is done for [1],[2]{2}- and [1],[2]{(00),2}-grazyne, which feature the strongest adsorptions for CO<sub>2</sub> and CH<sub>4</sub>, but not for [1],[1,2]{0,1}-grazyne, where the adsorption energies are smaller; i.e., at the working conditions where CO<sub>2</sub> and CH<sub>4</sub> would not adsorb on neither [1],[2]{2}- nor [1],[2]{(00),2}-grazyne, they definitely would not adsorb on [1],[1,2]{0,1}-grazyne. Fig. 11 shows the kinetic phase diagrams for [1],[2]{2}- and [1],[2]{(00),2}-grazyne (black and blue lines, respectively) defining the  $p/T$  conditions where CO<sub>2</sub> and CH<sub>4</sub> molecules are expected to pass across the membrane feasibly. From the kinetic phase diagram, it is clear that the [1],[2]{2}-grazyne allows CO<sub>2</sub> adsorption in a greater range than the [1],[2]{(00),2}-grazyne.

Aside, the CH<sub>4</sub> adsorption equilibrium lines are higher in pressure, implying that adsorbing CH<sub>4</sub> is much more difficult than CO<sub>2</sub>. In any case, the important aspect is that, e.g., at a standard pressure of 1 bar —10<sup>5</sup> Pa— and  $T = 300$  K, neither CO<sub>2</sub> nor CH<sub>4</sub> would be adsorbed, and, naturally, even less when having lower partial pressures. According to this, nano-engineered grayzane models would be not sweep materials for neither CO<sub>2</sub> nor CH<sub>4</sub>.

### 3.7. Comparison between materials

At this point, it is both interesting and worth to compare the studied grayzanes with other materials found in the literature in the context of biogas upgrading. Recently, DFT simulations of CO<sub>2</sub> capture using MXenes with the M<sub>2</sub>C stoichiometry obtained adsorption energies for CO<sub>2</sub> ranging from  $-2.11$  eV to  $-3.36$  eV and for CH<sub>4</sub> ranging from  $-0.13$  eV to  $-0.38$  eV [18]. As can be seen, very high energy values were obtained for CO<sub>2</sub> adsorption, being 13–26 times larger than for CH<sub>4</sub> and, unlike what happens with grayzanes, a chemisorption process was foreseen. In Ref. [18], CO<sub>2</sub> adsorption was important because the goal was focused on CO<sub>2</sub> capture and not on CO<sub>2</sub> filtration. Moreover, all MXenes featured extremely high selectivities at room temperature, being the highest and the lowest of the order of 10<sup>49</sup> and 10<sup>13</sup>, respectively. Clearly such MXene materials display a much higher selectivity compared to the present grayzanes, but at the expense of eventually having their surfaces saturated with CO<sub>2</sub>. Thus, for such materials the filtering process needs regeneration steps, to eliminate the adsorbed

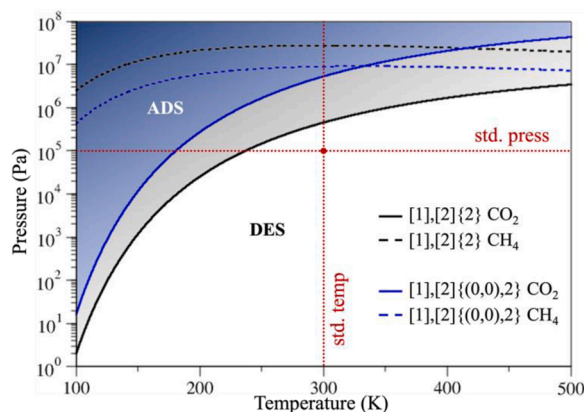


Fig. 11. Kinetic phase diagram of [1],[2]{2}-grazyne (black) and [1],[2]{(00),2}-grazyne (blue) as a function of CO<sub>2</sub> or CH<sub>4</sub> gases pressure and temperature. Fade zones denote working conditions where gases would be adsorbed, and the white one, conditions at which gases would desorb, leaving the grayzane sheet pristine. Red dotted lines indicate  $T = 300$  K and  $p = 1$  atm.

CO<sub>2</sub>, or CO and O fragments resulting from the CO<sub>2</sub> dissociation upon.

Another type of materials that obtained promising results in CO<sub>2</sub> capture are TMCs [5] with adsorption energies for CO<sub>2</sub> and CH<sub>4</sub> of  $-1.65$  eV and  $-0.77$  eV, respectively. Again, CO<sub>2</sub> proved to be more feasible of being captured by these materials, thus, purifying biogas. Furthermore, and as happened with MXenes, higher selectivities were obtained with TMCs ranging from 10<sup>5</sup> to 10<sup>19</sup>, but, at the same time, suffer from the same drawback; the necessity of regenerating the material for its re-use.

Finally, it is worth highlighting a study of biogas upgrading with multi-layered graphene nanostructures [6], so, in this sense more similar to this study on grayzanes. Ref. [6] shows relatively high selectivities of CO<sub>2</sub> over CH<sub>4</sub> at 35 and 100 bars and at 298.15 K. Actually, they found the highest selectivity value of 3500 and 3000 approx. for 100 and 35 bar, respectively, which are excellent, but having the handicap of needing to work at extremely high pressures. Normally, activated carbon is regarded as a referent, scrubbing material, with a higher affinity towards CO<sub>2</sub> than for CH<sub>4</sub>, which leads to enrichment values of ca. 86% [27].

The relatively small physisorption of CO<sub>2</sub>, of about  $-0.03$  eV as DFT computed [27], makes activated carbon (AC) to display a good CO<sub>2</sub> removal efficiency, with low energy requirements for regeneration [28, 29], at variance with the above commented MXenes and TMCs. Indeed, amine modified AC or porous silica have been targeted for CO<sub>2</sub>/CH<sub>4</sub> improved separation [28,30], and so periodic mesoporous phenylene-silicas [31]. However, their main disadvantage is the relatively low CO<sub>2</sub> capture capacity, of the order of mmol g<sup>-1</sup> [28,30–32], and the necessity to work under swing conditions of capture and regeneration. Here grayzanes would allow for a continuous separation, and, *a priori*, a larger separated quantity per unit mass, but to better assess whether the studied grayzane models would be competitive to such materials backing up such statements, a MD analysis is carried out in the next section.

### 3.8. Molecular dynamics

From molecular dynamics, it has been possible to verify whether the results forecasted from DFT calculations are accurate, at least, qualitatively. Here, the grayzane membranes and gas mixtures are simulated, counting the number of gas molecules that manage to cross the grayzane membrane over time, and with this, it is possible to gain the permeability of the membrane for CO<sub>2</sub> and CH<sub>4</sub> molecules, according to Eq. (13). Fig. 12 shows the time evolution of the number of CO<sub>2</sub> molecules in the permeated side of the grayzane membranes at different total pressures, but always starting from equimolar mixtures of CO<sub>2</sub> and CH<sub>4</sub>. Notice that only [1],[2]{2}- and [1],[2]{(00),2}-grazyne structures are represented because [1],[1,2]{0,1}-grazyne showed to be completely

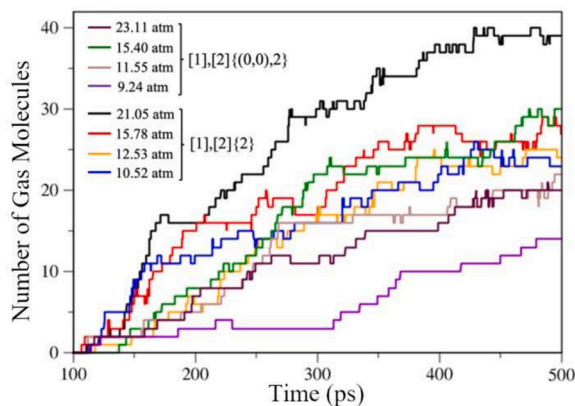


Fig. 12. Time evolution of the number of CO<sub>2</sub> molecules in the permeated side of [1],[2]{2}- and [1],[2]{(00),2}-grazyne at different pressures.

non-permeable to both molecules at all studied conditions due to the high diffusion barriers associated to both species.

Note that time evolution starts at 100 ps due to the first  $10^6$  iterations belong to the gas phase thermalization process where it was avoided the interaction of molecules with the membrane. Fig. 12 shows that the two grazylene structures represented are capable of filtering CO<sub>2</sub> through them and, as expected, the higher the pressure, the greater the number of CO<sub>2</sub> molecules in the permeated side, so far in full correlation with the aforementioned DFT estimates. Comparing the two compounds at similar pressures, there is no great difference in the number of filtered molecules. In the case of methane, it has been observed that only one molecule was able to cross the grazylene membrane in the [1],[2]{2}-grazylene at the four considered pressures, while for [1],[2]{(0,0),2}-grazylene no methane molecules were observed in the permeated side.

Comparing the performance of [1],[2]{2}-grazylene with experimental results of activated carbon found in the literature [29], the selectivity of such a grazylene at ca. 10 bar of 23 is at least 4.5 times larger than the selectivity of 5 found for AC at 293 K and at 70/30 (v/v) mixture of CH<sub>4</sub>/CO<sub>2</sub>. This superior selectivity is further increased for the [1],[2]{(0,0),2}-grazylene, which makes the presently studied grazynes as clearly improved C-based materials for biogas upgrading. Apart from the superior CO<sub>2</sub> selectivity, the pore permeation, and the absence of adsorption, *vide supra*, makes a continuous flux work viable, with the concomitant operation advantages. Last but not least, the permeated CO<sub>2</sub> on [1],[2]{2}-grazylene corresponds to an amount of 62.4 mmol of CO<sub>2</sub> g<sup>-1</sup>, almost an order of magnitude larger than a captured value of 8.2 mmol g<sup>-1</sup> on AC [29], and that gained at barely 0.5 nanoseconds, while the CO<sub>2</sub> capture experiments were carried out up to equilibrium reached after more than 120 min. Thus, permeation through such C-based grazylene membranes poses itself as a clearly better technology for biogas upgrading when comparing with biogas upgrading by CO<sub>2</sub> capture.

Coming back to the explicit present results, the number of crossed CO<sub>2</sub> and CH<sub>4</sub> molecules and the permeability are encompassed in Table 7 for [1],[2]{2}-grazylene, where it is clear that the CO<sub>2</sub> diffusion occurs in a much frequent way than that of CH<sub>4</sub>, being larger than in the [1],[2]{(0,0),2}-grazylene whose results are found in Table 8. Notice how the number of permeated CO<sub>2</sub> increases when the pressure is increased, correspondingly to its permeability, an observable trend shown in Fig. 13. It is noteworthy that even though CO<sub>2</sub> has not been completely isolated from CH<sub>4</sub> in this grazylene membrane, the CO<sub>2</sub> diffusion is clearly and highly favored. In this sense, it has been possible to compute the new purity of the upgraded biogas for each of the different pressures, obtaining purity improvements ranging from ca. 11–22 %.

A visual inspection of the MD simulation actually shows how the CO<sub>2</sub> molecule cross the membrane in a conformation similar to the perpendicular one, while CH<sub>4</sub> molecules simply bounce out when reaching the grazylene membrane. Definitely, the overall pressures are a way of controlling the CO<sub>2</sub>/CH<sub>4</sub> chemical separation, but one has to keep in mind that even if larger selectivity values would be achieved at lower pressures, that is done at the expense of smaller permeabilities. A balance in between two aspects feels necessary.

The same data analysis has been done for [1],[2]{(0,0),2}-grazylene in

**Table 7**

Number of gas molecules permeated and the permeability through [1],[2]{2}-grazylene at different pressures. The initial composition of the simulated biogas is 50 % methane admixed with 50 % CO<sub>2</sub>, and the resulting purity of methane after the upgrading is shown in %.

Pressure/atm	21.05	15.78	12.63	10.52
#CO <sub>2</sub>	39	27	24	23
#CH <sub>4</sub>	1	1	1	1
Purity (%)	71.9	63.3	61.5	61
$P_{CO_2}$	$2.47 \cdot 10^5$	$1.86 \cdot 10^5$	$1.28 \cdot 10^5$	$1.31 \cdot 10^5$
$P_{CH_4}$	$3.21 \cdot 10^3$	$3.21 \cdot 10^3$	$3.21 \cdot 10^3$	$3.21 \cdot 10^3$

**Table 8**

Number of gas molecules permeated and the permeability through [1],[2]{(0,0),2}-grazylene at different pressures. Resulting methane purity after upgrading is shown in percentage.

Pressure/atm	23.11	15.40	11.55	9.24
#CO <sub>2</sub>	20	30	14	12
#CH <sub>4</sub>	0	0	0	0
Purity (%)	59.3	65.3	56.1	55.2
$P_{CO_2}$	$9.86 \cdot 10^4$	$1.06 \cdot 10^5$	$7.74 \cdot 10^4$	$3.75 \cdot 10^4$
$P_{CH_4}$	—	—	—	—

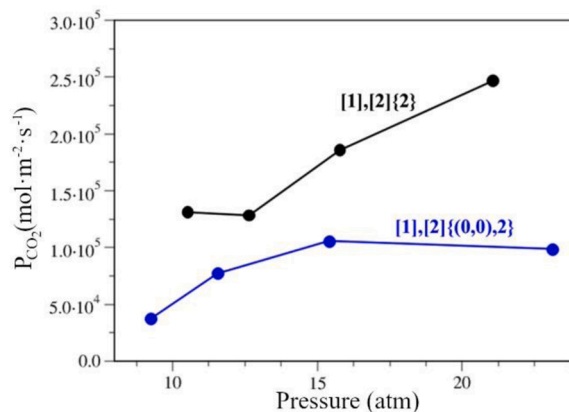


**Fig. 13.** Permeability of CO<sub>2</sub> on [1],[2]{2}-grazylene (black) and [1],[2]{(0,0),2}-grazylene (blue) at different gas stream pressures.

**Table 8.** The most remarkable thing about this membrane is to see that no CH<sub>4</sub> molecules have been able to cross the membrane for any pressure value throughout the simulations, so a 100 % pure CO<sub>2</sub> stream could be obtained. In any case, the high selectivity towards CO<sub>2</sub> agrees with what was obtained in CH<sub>4</sub> DFT calculations, where the [1],[2]{2}-grazylene obtained a lower diffusion energy barrier than that obtained by [1],[2]{(0,0),2}-grazylene, 0.22 eV and 0.31 eV, respectively, see Table 6. This energy difference is responsible for seeing methane passing through [1],[2]{2}-grazylene and not [1],[2]{(0,0),2}-grazylene. Thus, in order to observe the diffusion of larger molecules like CH<sub>4</sub>, the penetration energy barrier should be reduced somehow, either having larger pores, increasing CH<sub>4</sub> pressure, or changing the grazylene either geometry or electronic structure so as to lower the repulsion between substrate and adsorbate (methane), particularly in the transition state. As done for the [1],[2]{2}-grazylene, the biogas is enriched by 5–15 %, confirming that the CO<sub>2</sub> diffusion is highly favored in this grazylene type, therefore being seemingly a suitable compound for biogas upgrading.

After such promising, the trend towards enrichment has been evaluated regarding higher methane concentration biogas admixtures. In this sense, two MD simulations have been carried out with CH<sub>4</sub> concentrations of 75 % or 95 % (v/v) at 23.11 atm of pressure and 500 ps of simulation time. Results lead, for the first case, to 13 CO<sub>2</sub> molecules out of 32 trespassing the membrane, implying biogas upgrading up to 83.5% in CH<sub>4</sub>, thus obtaining an improvement beyond 8 %. For the 95 % CH<sub>4</sub> (v/v) simulation, a molecule out of six managed to pass through the grazylene, resulting in an improvement of ca. 1 % compared to the initial concentration, but, more importantly, pointing out that biogas upgrading can be carried out beyond the sought 95% (v/v) case using such grazynes as membranes. Obviously, these percentages would get even better at longer simulations, yet at a higher computational cost.

Leaving aside the more quantitative results and visualizing the obtained trajectories as a result of the molecular dynamics simulations, a trend has been observed that is followed by all the MD simulations for all the studied grazylene membranes. This deals with the movement that the grazylene membrane features when it interacts with the adsorbate

molecules. It has been observed that the grazyne bulges along the vacuum direction as if there would be a wave, see Fig. 14. Actually, some atoms are fixed at the material edge to avoid the drifting, so the material could be basically pushed by the gas pressure. However, the grazyne bulging is appearing regardless of the applied pressure. Apart from this, Fig. 14 shows gas molecules after the thermalizing process and a snapshot showing some CO<sub>2</sub> molecules crossing the membrane after the diffusion process is allowed.

#### 4. Conclusions

Having analyzed the biogas upgrading by grazyne, regarding thermodynamics and kinetics by static DFT calculations, and the dynamics through MD simulations, a series of important, grounded conclusions can be gained. First, it has been seen that, as the size of the acetylene pore increases, both adsorption and penetration barrier energies decrease for both CO<sub>2</sub> and CH<sub>4</sub>. The most significant change is actually seen for the diffusion barrier energy, given that when working with a larger pore, the repulsion in the transition state decreases. When considering two orientations for CO<sub>2</sub>, perpendicular and parallel, it has been observed that perpendicular CO<sub>2</sub> diffusion is favored energetically. In the transition state for the parallel orientation, the oxygen atoms of CO<sub>2</sub> were found closer to the grazyne membrane leading to a much greater interaction. Moreover, from the coverage analysis, it has been seen that the diffusion barrier is reduced up to ca. 0.30 eV in CO<sub>2</sub> cases halving the coverage. When one compares the results obtained for each grazyne compound, one gets from DFT calculations that [1],[2]{(00),2}-grazyne seems to be the most suitable to carry out the biogas upgrading process, given the fact that it features higher diffusion rates and selectivity. However, it must be borne in mind that a very high selectivity is not necessarily accompanied by a rapid diffusion rate, which is actually also mandatory for an effective use. Thus, a compromise is needed in between the two aspects for the studied grazyne membranes.

The molecular dynamics simulations confirmed that CO<sub>2</sub> molecules pass across [1],[2]{2}-grazyne and [1],[2]{(00),2}-grazyne membranes whereas methane has only been filtered in the [1],[2]{2}-grazyne. Even when featuring diffusion barriers below 1 eV, neither CO<sub>2</sub> nor CH<sub>4</sub> diffusion processes were observed on the [1],[1,2]{0,1}-grazyne case. This nevertheless underscores that lower energy barriers are needed to acquire significant permeabilities. Still, the gas stream pressure is found to be important in determining the number of molecules that will pass into the permeate part of the grazyne. Nevertheless, one has to keep in mind that increasing the pressure may lead to methane diffusing as well, reducing selectivity. However, low pressures yield lower permeabilities, so a compromise point seems to be mandatory. Finally, the permeability of [1],[2]{2}-grazyne for CO<sub>2</sub> has been found higher than the obtained in [1],[2]{(00),2}-grazyne, but, at the same time, it is also higher for CH<sub>4</sub>. Being the [1],[2]{(00),2}-grazyne totally rather impermeable for CH<sub>4</sub> and rather permeable for CO<sub>2</sub>, that would be the most suitable grazyne candidate for biogas upgrading, while MD simulations seem to point out [1],[1,2]{0,1}-grazyne as rather impermeable for both CO<sub>2</sub> and CH<sub>4</sub>. We deem it important to add that this study has not considered different impurities that can be found in raw biogas streams, such as H<sub>2</sub>S, NH<sub>3</sub>, or water, among others, which should be regarded in any proof of concept, addressing regenerability or degradation issues. Furthermore, such issues can affect the economic and environmental aspects of grazyne utilization, here still untreatable until the grazyne synthesis milestone has been reached, but that once is achieved and tested, will be a key aspect to be regarded for practical applications, as done in previous studies, e.g. as done in previous studies like the biogas generation from anaerobic digestion [33].

The present results pose nano-engineered grazyne membranes as suitable materials for biogas upgrading processes, based on the correlated DFT and MD simulations, and considering thermodynamic, kinetic, and dynamic aspects. Grazyne has quite interesting advantages with respect other materials such as TMCs and MXenes, being light

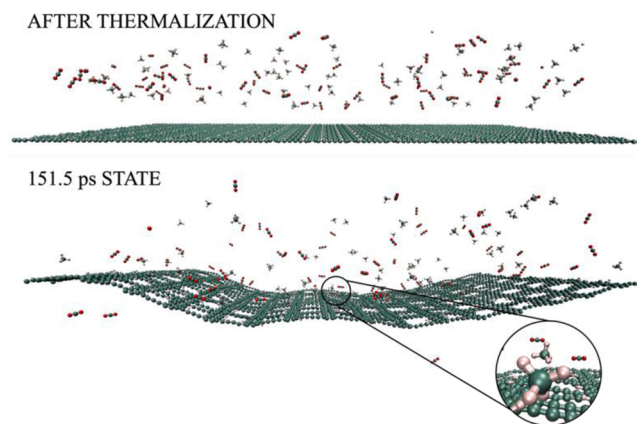


Fig. 14. MD snapshots for [1],[2]{(00),2}-grazyne membrane after thermalizing the gas mixture (top) and after 151.5 ps (bottom). Inset image corresponds to a close view of the interaction of some gas molecules with the membrane. Color coding as in Fig. 3.

materials, made from Earth abundant elements, and avoiding being sweep materials for neither CO<sub>2</sub> nor CH<sub>4</sub>, thus enabling for a continuous use, without the need of regenerating the material after certain working times. The present work puts grazyne materials in the biogas upgrading map, with different tuning capabilities to maximize the chemical separation to the sought 95% (v/v) of CH<sub>4</sub> content needed for biogas commercialization [4], by, e.g., considering other pores, or the possible effect of other capping agents on C dangling bonds, such as using fluorine or other halides. Aside, the sieving capacity is in the order of several dozens of CO<sub>2</sub> mmol g<sup>-1</sup> in the ns time scale, while sweeper materials such as those based on activated carbon achieve few mmol g<sup>-1</sup>, with less selectivity and reached after exposure for hours, thus posing grazyne membranes as a better technology for biogas upgrading. Last but not least, one could envisage other chemical resolution applications on the designed grazyne materials, for instance, separating CH<sub>4</sub> from H<sub>2</sub> after methanation synthesis process, where one could envisage pores with a quite easy diffusion of H<sub>2</sub>.

#### CRedit authorship contribution statement

**Francesc Viñes:** Conceptualization, Supervision, Formal analysis, Writing – review & editing, Resources, Funding acquisition, Project administration. **Pablo Gamallo:** Conceptualization, Supervision, Formal analysis, Writing – review & editing, Resources, Funding acquisition, Project administration. **Adrià Calzada:** Visualization, Validation, Investigation, Software, Data curation, Formal analysis, Writing – original draft.

#### Declaration of Competing Interest

The authors declare that they have no known competing financial interests or personal relationships that could have appeared to influence the work reported in this paper.

#### Data Availability

Data will be made available on request.

#### Acknowledgements

This study has been supported by the Spanish Ministry of Science and Innovation (MICIN) through the projects MCIN/AEI/10.13039/501100011033, RTI2018-094757-B-I00, RTI2018-095460-B-I00, and PID2021-126076NB-I00, funded partially by FEDER *Una manera de hacer Europa*, the CEX2021-01202-M María de Maeztu Unit of

Excellence, and the MCIN/AEI/10.13039/501100011033 PID2020-115293R-I00. P.G. thanks Generalitat de Catalunya for his Serra Hunter Associate Professorship.

## References

- [1] Intergovernmental Panel on Climate Change, *Climate Change 2021: The Physical Science Basis*, IPCC, 2021.
- [2] *World Energy Outlook 2021*, International Energy Agency (IEA), 2021.
- [3] F. Meng, Y. Meng, T. Ju, S. Han, L. Lin, J. Jiang, Research progress of aqueous amine solution for CO<sub>2</sub> capture: a review, *Renew. Sustain. Energy Rev.* 168 (2022), 112902.
- [4] Q. Sun, H. Li, J. Yan, L. Liu, Z. Yu, X. Yu, Selection of appropriate biogas upgrading technology – a review of biogas cleaning, upgrading and utilization, *Renew. Sustain. Energy Rev.* 51 (2015) 521–532.
- [5] C. Kunkel, F. Viñes, F. Illas, Biogas upgrading by transition metal carbides, *ACS Appl. Energy Mater.* 1 (2018) 43–47.
- [6] J.J. Chen, W.W. Li, X.L. Li, H. Yu, Improving biogas separation and methane storage with multilayer graphene nanostructure via layer spacing optimization and lithium doping: a molecular simulation investigation, *Environ. Sci. Technol.* 46 (2012) 10341–10348.
- [7] I. Covarrubias-García, G. Quijano, A. Aizpuru, J.L. Sánchez-García, J.L. Rodríguez-López, S. Arriaga, Reduced graphene oxide decorated with magnetite nanoparticles enhance biomethane enrichment, *J. Hazard. Mater.* 397 (2020), 122760.
- [8] A.T. Balaban, C.C. Rentea, E. Ciupitu, Chemical graphs VI. Estimation of the relative stability of several planar and tridimensional lattices for elementary carbon, *Rev. Roum. Chim.* 13 (1968) 231–247.
- [9] D. Malko, C. Neiss, F. Viñes, A. Görling, Competition for graphene: graphynes with direction-dependent Dirac cones, *Phys. Rev. Lett.* 108 (2012) 8–24.
- [10] Z. Li, M. Smeu, A. Rives, V. Maraval, R. Chauvin, M.A. Ratner, E. Borguet, Towards graphyne molecular electronics, *Nat. Commun.* 6 (2015) 6321.
- [11] Y. Hu, C. Wu, Q. Pan, Y. Jin, Y. Lyu, V. Martínez, S. Huang, J. Wu, L.J. Wayment, N. A. Clark, M.B. Raschke, Y. Zhao, W. Zhang, Synthesis of  $\gamma$ -graphyne using dynamic covalent chemistry, *Nat. Synth.* 1 (2022) 449–454.
- [12] S. Kamalinahad, F. Viñes, P. Gamallo, Grazyne: carbon-based two-dimensional composites with anisotropic properties, *J. Phys. Chem. C* 123 (2019) 27140–27149.
- [13] I. Alcón, N. Papior, G. Calogero, F. Viñes, P. Gamallo, M. Brandbyge, Acetylene-mediated electron transport in nanostructured graphene and hexagonal boron nitride, *J. Phys. Chem. Lett.* 12 (2021) 11220–11227.
- [14] G. Kresse, J. Furthmüller, Efficiency of ab-initio total energy calculations for metals and semiconductors using a plane-wave basis set, *Comput. Mater. Sci.* 6 (1996) 15–50.
- [15] P.E. Blöchl, Projector augmented-wave method, *Phys. Rev. B* 50 (1994) 17953–17979.
- [16] J.P. Perdew, K. Burke, M. Ernzerhof, Generalized gradient approximation made simple, *Phys. Rev. Lett.* 77 (1996) 3865–3868.
- [17] S. Grimme, J. Antony, S. Ehrlich, H. Krieg, A consistent and accurate ab initio parametrization of density functional dispersion correction (DFT-D) for the 94 elements H–Pu, *J. Chem. Phys.* 132 (2010), 154104.
- [18] H. Prats, H. Mcaloon, F. Viñes, F. Illas, Ultra-high selectivity biogas upgrading through porous MXenes, *J. Mater. Chem. A* 8 (2020) 12296–12300.
- [19] S. Plimpton, P. Crozier, A. Thompson, LAMMPS – large-scale atomic/molecular massively parallel simulator, Sandia Natl. Lab. (2007).
- [20] J.S. Stuart, A.B. Tutein, J.A. Harrison, A reactive potential for hydrocarbons with intermolecular interactions, *J. Chem. Phys.* 112 (2000) 6472–6486.
- [21] B. Vujčić, A.P. Lyubartsev, Transferable force-field for modelling of CO<sub>2</sub>, N<sub>2</sub>, O<sub>2</sub>, and Ar in all silica and Na<sup>+</sup> exchanged zeolites, *Model. Simul. Mater. Sci. Eng.* 24 (2016), 045002.
- [22] A. Calzada, *Molecule Counter* program, 2022. [https://github.com/AdriaCalzada/MolecularDynamics/blob/main/molec\\_counter.f](https://github.com/AdriaCalzada/MolecularDynamics/blob/main/molec_counter.f).
- [23] H. Du, J. Li, J. Zhang, G. Su, X. Li, Y. Zhao, Separation of hydrogen and nitrogen gases with porous graphene membrane, *J. Phys. Chem. C* 115 (2011) 23261–23266.
- [24] S. Kim, P. Gamallo, F. Viñes, J.Y. Lee, The nano gold rush: graphynes as atomic sieves for coinage and Pt-group transition metals, *Appl. Surf. Sci.* 499 (2020), 143927.
- [25] A. Nicolai, B.G. Sumpter, V. Meunier, Tunable water desalination across graphene oxide framework membranes, *Phys. Chem. Chem. Phys.* 16 (2014) 8646–8654.
- [26] Á. Morales-García, M. Mayans-Llorach, F. Viñes, F. Illas, Thickness biased capture of CO<sub>2</sub> on carbide MXenes, *Phys. Chem. Chem. Phys.* 21 (2019) 23136–23142.
- [27] L. China, K. Słowiecka, P. Bartocci, A.-H. Alissa Park, S. Wang, D. Jiang, F. Fantozzi, Methane enrichment of biogas using carbon capture materials, *Fuel* 334 (2023), 126428.
- [28] M.R. Al Mamun, M.R. Karim, M.M. Rahman, A.M. Asiri, S. Torii, Methane enrichment of biogas by carbon dioxide fixation with calcium hydroxide and activated carbon, *J. Taiwan Inst. Chem. Eng.* 58 (2016) 476–481.
- [29] P.C. Vilella, J.A. Lira, D.C.S. Azevedo, M. Bastos-Neto, R. Stefanutti, Preparation of biomass-based activated carbons and their evaluation for biogas upgrading purposes, *Ind. Crops Prod.* 109 (2017) 134–140.
- [30] L. Mafra, T. Cendak, S. Schneider, P.V. Wiper, J. Pires, J.R.B. Gomes, M.L. Pinto, Amine functionalized porous silica for CO<sub>2</sub>/CH<sub>4</sub> separation by adsorption: which amine and why, *Chem. Eng. J.* 336 (2018) 612–621.
- [31] M.A.O. Lourenço, C. Siquet, M. Sardo, L. Mafra, J. Pires, M. Jorge, M.L. Pinto, P. Ferreira, J.R.B. Gomes, Interaction of CO<sub>2</sub> and CH<sub>4</sub> with functionalized periodic mesoporous phenylene-silica: periodic DFT calculations and gas adsorption measurements, *J. Phys. Chem. C* 120 (2016) 3863–3875.
- [32] R.B. Rios, F.M. Stragliotto, H.R. Peixoto, A.E.B. Torres, M. Bastos-Neto, D.C. S. Azevedo, C.L. Cavalcante Jr., Studies on the adsorption behavior of CO<sub>2</sub>-CH<sub>4</sub> mixtures using activated carbon, *Braz. J. Chem. Eng.* 30 (2013) 939–951.
- [33] L. Wu, W. Wei, L. Song, M. Woźniak-Karczewska, L. Chrzanowski, B.-J. Ni, Upgrading biogas produced in anaerobic digestion: biological removal and bioconversion of CO<sub>2</sub> in biogas, *Renew. Sustain. Energy Rev.* 150 (2021), 111448.